Ship maneuvering simulation with CFD approach

Ganbo Deng, Patrick Queutey, Emmanuel Guilmineau, Alban Leroyer, Michel Visonneau, Jeroen Wackers

Ship maneuvering simulation with CFD approach

G. Deng[a], P. Queutey[b], A. Leroyer[c], E. Guilmineau[d], M. Visonneau[e], J. Wackers[f]

a. Ecole Centrale de Nantes, Ganbo.Deng@ec-nantes.fr
b. Ecole Centrale de Nantes, Patrick.Queutey@ec-nantes.fr
c. Ecole Centrale de Nantes, Alban.Leroyer@ec-nantes.fr
d. Ecole Centrale de Nantes, Emmanuel.Guilmineau@ec-nantes.fr
e. Ecole Centrale de Nantes, Michel.Visonneau@ec-nantes.fr
f. Ecole Centrale de Nantes, Jeroen.Wackers@ec-nantes.fr

Résumé :

Ce papier est consacré à l'évaluation de la simulation de manœuvrabilité de bateau par l'approche CFD avec l'accent mis sur un modèle simplifié de l'hélice pour lequel l'action de cette hélice est représentée par un champ de force dont la densité est déterminée par la charge du bateau pendant sa manœuvre à l'aide de la courbe de performance de l'hélice en eau libre. A titre de comparaison, des simulations avec une hélice tournante par l'approche RANSE ont été également effectuées. Deux approches ont été comparées pour ces dernières simulations : une méthode précise en temps à l'aide d'interfaces glissantes et une simulation effectuée dans un repère tournant pour prendre en compte la rotation de l'hélice. Des manœuvres en zigzag et en mouvement circulaire ont été simulées pour deux bateaux différents, à savoir le modèle ONRT et le modèle KCS. Les résultats des simulations ont été comparés aux résultats expérimentaux afin d'évaluer la performance de la simulation numérique avec l'approche RANSE obtenue à partir de modèles différents pour l'hélice.

Abstract :

This paper is devoted to the assessment of ship maneuvering simulation with CFD approach using different propeller models with a focus on a simplified propeller model that represents the action of the propeller by body force and uses propeller performance curve to determine propeller loading during ship maneuvering. Simulations are also performed with an actual propeller approach with which the propeller rotation is simulated directly with the RANSE solver. Both time accurate simulations using sliding grid and rotating frame approximations have been performed for comparison. The zigzag and turning circle maneuvers in calm water have been simulated for two different ship models, namely the ONRT test case and the KCS test case. Predicted ship motion is compared with measurement data to assess the accuracy of the numerical prediction using RANSE computations with different propeller models.

Mots clefs : Ship zigzag and turning circle motion, simplified propeller model with body force, actual propeller approach

1 Introduction

CFD can be considered as a mature tool now for steady state ship hydrodynamic applications such as resistance in calm water. Accurate enough predictions can be obtained with reasonable resources even for fully appended hulls, both for model and full scale in a routine design procedure. Self propulsion computation can also be performed easily with the same cost if a simplified propeller model based on body force is used. More accurate predictions can be obtained by simulating directly the rotating propeller with sliding or overset grids. For an unsteady application without propeller, such as sea-keeping and PMM maneuvering motion, simulation can still be performed with affordable computational resources, typically a few days wall clock time with 100 to 200 cores. The situation is different for unsteady flow simulation including a rotating propeller such as zigzag and turning circle maneuvering motion. The most accurate approach for such a configuration is to simulate the rotating propeller directly with the RANSE solver. It is usually called discrete propeller approach or actual propeller approach. Since time accurate simulation is required for such simulation and the time step needed to resolve the rotating propeller is very small, such a computation is often very expensive. One month wall clock time or even more is needed using 100 to 200 cores. To reduce the CPU cost, a propeller model based on body force needs to be used. This will add an additional source of error due to the propeller model. In addition to the above mentioned difficulties related to the propeller, the accurate prediction of ship maneuvering motion is more difficult due to the flow separation around the rudder with high deflection angle and the formation of longitudinal vortex due to drift angle. Nowadays, it is not possible to draw a conclusion based on the published results concerning the predictive capability of CFD simulations for such application. The main objective of the present study is to perform CFD simulation for ship maneuvering application with and without propeller model and compare the result with the measurement data so that different sources of error can be identified.

Our experiences from various V&V exercises show that a reliable numerical uncertainty estimation in the case of 3D unsteady flow as considered here is nearly impossible due to high iterative error as well as time discretization error. Due to high computational cost, no attempt is made to assess space and time discretization error. Instead, the time step as well as the grid density for the original grid (suited for the implemented adaptive grid refinement) in various domains (hull, propellers, rudders, etc.) are chosen according to our experience in numerical settings for resistance tests and open water simulations in workshops and collaborative studies [1],[2],[3],[4].

2 Numerical approach

The flow solver ISIS-CFD developed by our team, available as a part of the FINE/Marine computing suite distributed by Cadence Design Systems, is an incompressible unsteady Reynolds-averaged Navier-Stokes (URANS) method mainly devoted to marine hydrodynamics. The method features several sophisticated turbulence models : apart from the classical two-equation k-ω models, anisotropic two-equation Explicit Algebraic Reynolds Stress Model (EARSM), as well as Reynolds Stress Transport Models. Hybrid RANS-LES turbulence models based on variants of Detached Eddy Simulation closures (DES-SST, DDES-SST, IDDES) are also implemented.

The solver is based on the finite volume method to build the spatial discretization of the transport equations. The unstructured discretization is face-based. While all unknown state variables are cell-centered, the systems of equations used in the implicit time stepping procedure are constructed face by face. Fluxes are computed in a loop over the faces and the contribution of each face is then added to the two cells

next to the face. Therefore, the grids can be completely unstructured ; cells with an arbitrary number of arbitrarily-shaped faces are accepted.
Pressure-velocity coupling is enforced through a Rhie & Chow SIMPLE type method : at each time step, the velocity updates come from the momentum equations and the pressure is given by the mass conservation law, transformed into a pressure equation. In the case of turbulent flows, transport equations for the variables in the turbulence model are added to the discretization. Free-surface flow is simulated with a multi-phase flow approach : the water surface is captured with a conservation equation for the volume fraction of water, discretized with specific compressive discretization schemes [5],[6]. Time-integration of Newton's law to solve the six d.o.f. for ship motion is described in [7].
To enable relative motions of appendages, propellers or bodies, sliding and/or overlapping grid approaches have been implemented. Propellers can be modeled using actuator disk theory, by coupling with boundary element codes or any other simplified propeller models. It can also be handled by direct discretization of the real propeller through e.g. the rotating frame method or sliding interface approaches [8],[9]. Finally, an anisotropic adaptive grid refinement (AGR) procedure has been developed which is controlled by various flow-related criteria. It is also used to improve the accuracy of overset interpolations as it automatically smooth out the cell sizes distribution across overset interfaces between domain [10],[11].
Parallelization is based on domain decomposition. The grid is divided into different partitions. The interface faces on the boundaries between the partitions are shared between the partitions ; information on these faces is exchanged with the MPI (Message Passing Interface) protocol. This method works with the sliding/overlapping grid approaches and the different sub-domains can be distributed arbitrarily over the processor cores without any loss of generality. Moreover, the AGR procedure is fully parallelized with a dynamic load balancing working transparently with or without sliding or overlapping grids.

3 Simplified propeller model

When a body force approach is used to simulate the propeller, the propeller model is critical for the accuracy of the simulation. The simplified propeller model used in the present study is inspired by the coupling procedure between RANSE and Boundary Element Method (BEM) solvers for propeller modelization. The RANSE/BEM coupling procedure is implemented in the following way. First, the RANSE solver provides the velocity field in front of the propeller as total velocity to the BEM code. The potential code computes the propeller induced velocity at the same position and deduces the effective wake. The effective wake is used as boundary condition in the BEM code to compute the propeller performance and represent the action of the propeller by body forces. Those body forces are then added as source term in the momentum equation for the RANSE simulation. There are two different ways to run the BEM code. It can perform a steady computation. In this case, the effective wake is averaged in the circumferential direction, so is the body force. The advantage of such computation is that the CPU cost is very low, typically a few seconds. But the result is less accurate. To obtain a better accuracy, an unsteady computation needs to be performed using the effective wake directly without averaging. Body force is averaged in time only. The key issue in this coupling procedure is how to accurately determine the effective wake in the propeller plane. Since the propeller induced velocity is computed by the BEM code, the body force needs to be represented as accurately as possible. Besides, the coupling plane is located in front of the propeller. To obtain the effective wake in the propeller plane, additional approximation is needed. We can replace the BEM code by the propeller performance curve to obtain a simple propeller model. This simple propeller model is implemented in a similar way as in a RANSE/BEM coupling

approach. The RANSE solver computes the mean velocity at the propeller plane. Another RANSE open water computation with body force is performed to obtain the propeller induced velocity. This open water RANSE computation can be performed independently. The propeller induced velocity can then be obtained by interpolation from the results of open water RANSE computation. Subtracting the mean velocity at the propeller plane from the propeller induced velocity will give us the propeller advancing speed. With the propeller advancing speed, we can determine the propeller thrust and torque from the propeller performance curve. Body forces are added in the source term of the momentum equation by using an empirical force distribution. This approach is not as accurate as a BEM code, since the effective wake distribution as well as the direction of the inflow velocity can not be taken into account. The advantage of this propeller model is its simplicity. It is only needed to provide a propeller performance Kt-Kq curve. There is no additional cost in the simulation. Propeller geometry is not needed except for the open water computation to obtain this Kt-Kq curve. In our present study, open water measurement data is used for this input. However, the drawbacks of this propeller model are the following. It responds to the mean axial velocity only. Non-uniform wake distribution as well as oblique inflow angle can not be taken into account. Moreover, only axial and tangential forces are taken into account. Side force effect is missing. Besides, forces are averaged in the circumferential direction, which may have an impact on the rudder operating behind the propeller.

4 Case setup

4.1 ONRT ship model

The ONR Tumblehome (ONRT) ship hull model, length Lpp = 3.147m, Fig. 1, is appended with a skeg and bilge keels. The model has also twin rudders, shafts and two 4-bladed propellers with shaft brackets. The rudders are of the spade type. The propellers are fixed pitch type with the direction of rotation inward over the top. It is the 5.2 test case of the SIMMAN workshop initially scheduled for 2019. Main par-

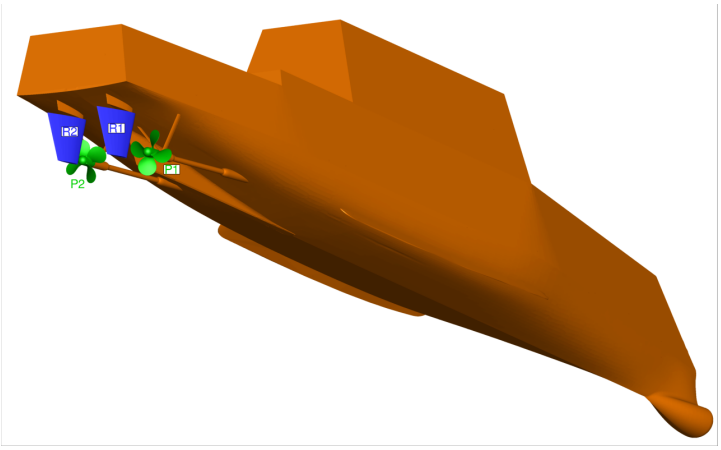

FIGURE 1 – The ONRT ship model

ticulars are described in http ://www.simman 2019.kr/contents/test_case_5.2.php and are not included here again for the sake of brevity. This reference contains also all the recommendations to simulate the $20°/20°$ starboard (SB) side zigzag maneuver in calm water starting with a first step exercise to evaluate the self-propulsion point at Fr=0.20 (target speed U=1.11m/s).
The choice of the mass m, inertia matrix I and location of the center of gravity as close as possible to the

experimental conditions is critical to solve the 6 d.o.f. for simulations. Our choice comes first from the prescribed draft 0.112m. Therefore the closed solid bodies (Fig.1) gives the numerical mass 73.7582 kg and CG coordinates=(1.625m, 0m, 0.044m) so that the numerical model is in equilibrium at rest (water density 999.19 kg/m^3). The reference frame is such that the bow is at x=0m with x-axis pointing towards AP and z=0 defines the plane of free-surface at rest. Serious doubts were raised after the Tokyo 2015 workshop about the value of kxx coefficient which define Ixx (m.kxx^2). From numerical roll damping in calm water at zero advance speed in the context of NATO/AVT-280 collaborative research project, we retained kxx=0.34B (ship breadth B=0.384m) which appears to be a reasonable choice to us (computed roll period 1.61s) compared with the original 0.44B (computed roll period 1.81s), close to the 0.344B proposed now in case 5.2 of the workshop. For the other coefficients Iyy and Izz (yaw and pitch), we keep the proposed radius 0.246xLpp.

Overset grid is used to handle ship free motion. A small ship domain is free to move with rigid mesh motion inside a background domain. Additional domains are created for the two propellers and for the two rudders. There is a total of six domains to be meshed independently by HEXPRESS, which results in a unique grid to be partitioned.

If sliding interfaces are considered between the ship and the propeller domains, overset interpolation is preferred between the ship domain and the background domain, and between the rudder and the ship domains. AGR is therefore very advantageous to minimize the interpolation errors across these interfaces. Figs. 2 and 3 are illustrative of the grid behavior during the zigzag maneuver in a constant-z or -x plane passing through the propeller center. In each domain the grid moves rigidly : rotating motion around the propeller axis or around the rudder axis.

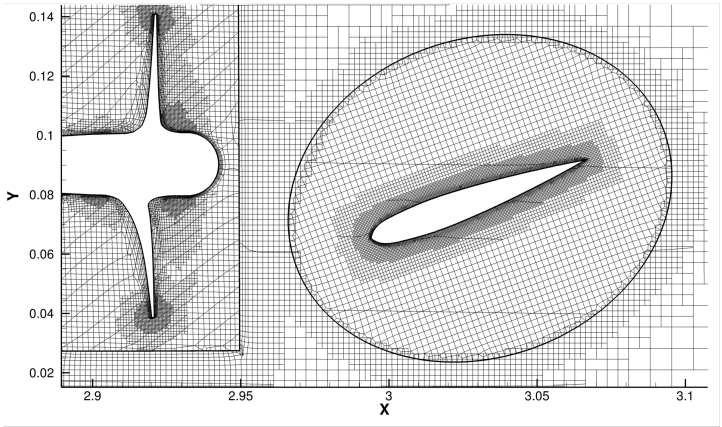

FIGURE 2 – Adapted grid in horizontal plane and close to propeller and rudder at an arbitrary time instant

As our objective is not to precisely simulate the experimental basin with influence of its walls, the background domain is moving but recovers only the (x,y) translations and the yaw of the ship d.o.f.. Inside the background domain, the ship domain is free to move, still rigidly, according to the roll, pitch and heave motions. Again, AGR is used to ensure the accuracy of the overset interpolations between the ship and the background domain and also to improve the interface capturing (with the help of combined criteria). The background domain extension is [-20m, 20m]x[-10m, 10m]x[-2Lpp, 0.5Lpp] with far-field boundary conditions on its vertical planes and prescribed pressure on top and bottom. Wall-function (target y+ about 40) is applied on all surfaces of the ship model.

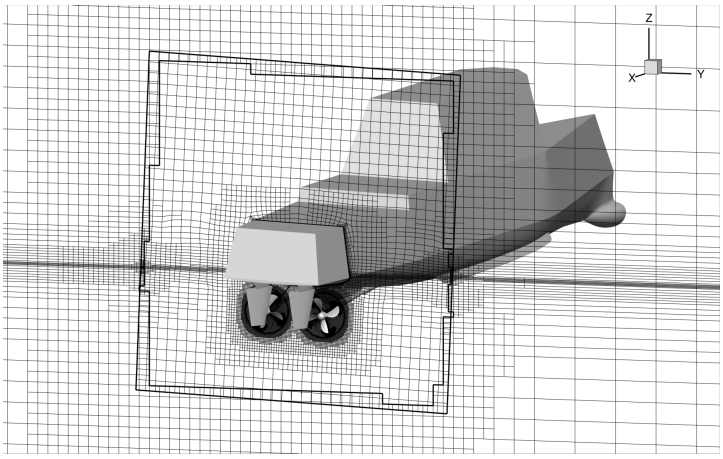

FIGURE 3 – Adapted grid in longitudinal plane through propeller centers at an arbitrary time instant

4.2 KCS ship model

This is the test case 3.2 of the SIMMAN 2019 workshop. The scale factor of the ship model is 37.89, giving a Lpp=6.07m. The target speed is 2.005m/s with a Froude number Fr=0.26. Unlike the previous case, a big ship domain is used without having recourse to a background domain. An overset domain is used for the rudder, while a sliding grid domain is used for the propeller for the actual propeller approach. The ship domain extension is [-19.2m, 19.2m]x[-12m,12m]x[-7.79m,3.41m]. The mid ship is located at x=0. For the computation using body force, the ship domain and the rudder domain contain 4.17M and 1.81M cells respectively, while for the case with actual propeller, there are 4.59M, 1.12M and 1.26M cells in the ship domain, rudder domain and the propeller domain, respectively. During the computation, AGR adds about 30% more cells to capture the free surface as well as to ensure cell size continuity near the overset interface. The geometry of the KCS ship model used in the CFD simulation is shown in figure 4. The propeller is separated from the hull with a gap so that both the ship and the propeller form a closed body. Hence, the force acting on the hull can be compared directly between different propeller models.

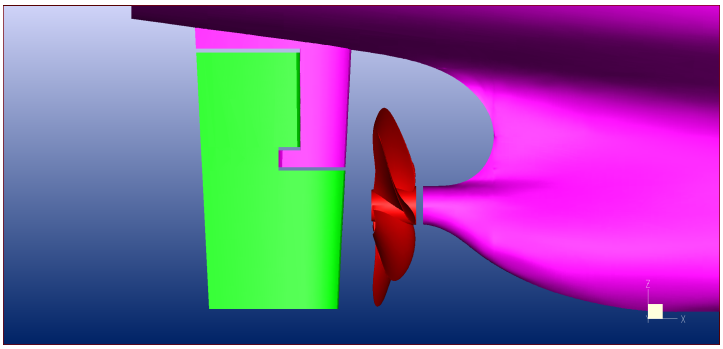

FIGURE 4 – The KCS ship model

5 Numerical setting and models

As stated in the introduction, the main objective of the study is to question if the use of simplified propeller model is a cost-effective alternative to full modeling where the only uncertainty would be the

turbulence modeling. To this purpose, we considered three approaches :
AD model : it is the body force approach with actuator disk model where the Kt-Kq curves from open water (EFD or CFD) are used to update the thrust and torque during the simulation when the propeller rps is imposed, or to determine the propeller rps in a self-propulsion simulation. The time step is similar to the time step used for resistance in calm water, typically 0.5*Lpp/U/100 rounded to 0.01s.
RFM model : the rotating frame method in ISIS-CFD is used to model a general rigid-body motion (rotation) where the RANS equations are solved in the moving reference frame but written in terms of absolute or inertial frame quantities. For example, it allows a steady calculation in case of open-water propeller or when the flow is steady in the moving frame. The time step used is therefore the same as for the reduced AD model, i.e. 0.01s.
AP model : the actual propeller is solved to provide a reference solution. The time step is therefore driven by the rps of the propeller (typically 2° per time step). For the ONRT test case, with a propeller revolution rate about 9 rps, the time step is about 0.0006s, 17 times smaller than AD or RFM models. For the KCS test case, since the time step used for the computation for the AD model is twice as bigger (0.02s), and the propeller rps is higher (about 12 rps), the time step ratio is 46. Then the AP model CPU cost is expected to be approximately 17 times and 46 times more expensive than with simplified propeller models for the ONRT and the KCS test case, respectively.
For the ONRT test case, the propeller is meshed for RFM and AP models. In the computation with body force, the blades in the propeller domain are removed, the propeller domain containing only the shaft. This way simplifies the mesh generation and only two original grids are used for all the simulations, see Table 1. In both cases, the target vertical size in the original grid around the free-surface at rest is Lpp/500 (7.5mm).

Domain/Model	RFM or AP	AD
Background	1,432,364	1,432,364
Ship	4,432,597	4,430,071
1 Propeller	1,151,019	725,472
1 Rudder	2,263,062	2,263,062
Total	12,693,123	11,729,503

TABLE 1 – Original mesh sizes in different domains

6 Results and discussions

6.1 ONRT self-propulsion step

The maneuver is performed at a fixed rps evaluated from a self-propulsion simulation. The rps depends on the model used AD, RFM or AP.
AP and RFM models : to find the revolution rate of the propellers corresponding to the target speed of the ship in calm water U=1.11 m/s, two simulations are conducted around the 8.97rps known from EFD, one 15% higher and the second 10% lower. In these simulations in calm water, only heave and pitch are solved and rudders are fixed. When the forces for ship resistance and the propeller thrust are established, the towing force for each simulation is deduced by the difference between the ship resistance and the propeller thrust. The self-propulsion point for which the towing force is zero is determined by linear interpolation between the above two operation points. The RFM approach is surprisingly closer to EFD

with 8.97rps than the AP model with 8.73rps (4.4% error). However, the good RFM prediction could be explained by the fact that the propellers are positioned laterally and do not operate directly in the wake of the ship. The self-propulsion point with the AD model is found directly by adjusting the body force coupled with the Kt-Kq curves during the simulation and prediction is 8.93rps (0.5% error) .

6.2 ONRT $20°/20°$ starboard side zigzag motion

For each model, simulation is simply restarted from the self-propulsion step releasing this time all six d.o.f and rudder motion such that the rudder rate is $35°/s$ with direct control from the computed yaw according to the zigzag rules, see Fig. 5 for notations. Due to available CPU resources only the SB zig-

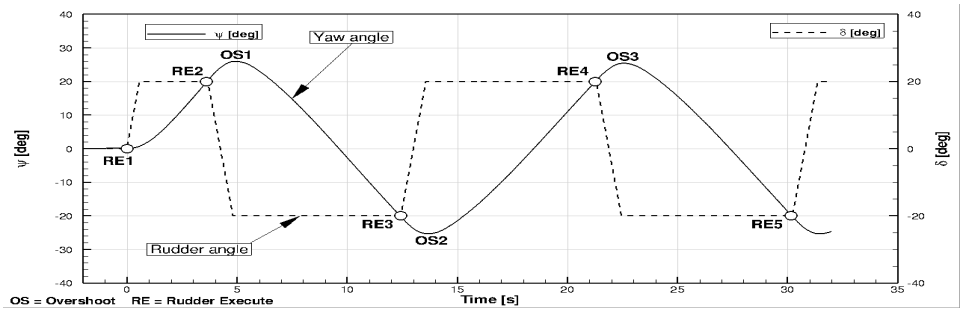

FIGURE 5 – $20°/20°$ zigzag rules and notations where RE means Rudder Execute, OS for overshoot of the computed ship's yaw ψ and δ is the controlled rudder angle.

zag for a total duration of 25s to 30s in physical time is considered. Parallel simulations are performed over 168 partitions for RFM and AP models and 160 for AD model. Simulations have been performed in one shot only without trying to optimize the CPU but keeping very conservative criteria to prioritize the quality of resolution (for linear systems and iterative coupling). If AD model is taken as a reference with a total CPU cost of 8,000 hours (2 days wall clock time) for 2,500 time steps, RFM cost is nearly the same with about 1.3 time the AD model but, as expected, the AP model cost with 40,000 time steps is 16.5 times higher (about 1 month wall clock time).

The time history of the relative increase of the number of cells from the original grid with AP is plotted in Fig. 6 where some significant aspects of the zigzag manoeuver (RE and OS) are indicated. Time 0 is the time of the first RE after a restart from the self-propulsion step. It shows that the most important efforts produced by AGR (by only 15%) are between two consecutive RE actions : from the ship and rudder motions and also from the free-surface changes where the vertical resolution of the anisotropic refinement goes until 1.8mm (a factor 4 from the original grid). Fig. 6 already shows that a periodic state of the zigzag motion seems to be already established after the first OS.

Results of post-processing of trajectory and time histories of some d.o.f. are compared between different propeller models and also to available EFD measurements [12][13]. EFD data from [12][13] have been simply digitized and therefore must be taken as such. These EFD data are used as an indication to qualify the propeller models. In all the following figures, the scanned measurements are represented by points and the result of the simulations by curves. The trajectory of the ship in Fig. 7 is the motion of the mid-ship point O(x(t),y(t),z=0). AP and AD models are in line with EFD with a slight improvement for AP. RFM method leads to an increasingly stretched trajectory along x.

This is consistent with the ship speed history, Fig. 8, as the surge and the sway velocities from RFM are over- and underestimated, respectively. The most negative effect of RFM is too low a sway velocity. The drawback of the RFM approach can be attributed to the fact that the propeller side force is poorly

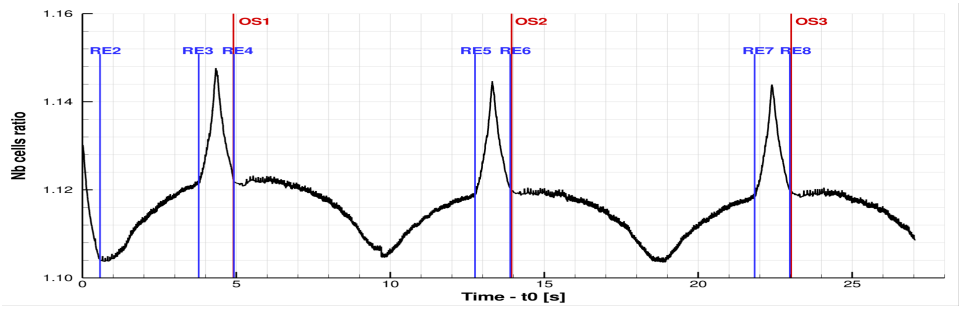

FIGURE 6 – Time history of the increase in cell number with AP model.

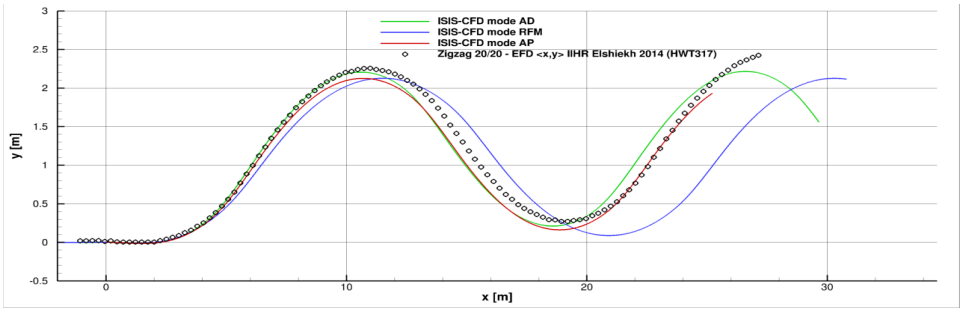

FIGURE 7 – Trajectory of the ship mid-point O in horizontal plane (x,y)

predicted since the propeller blades are frozen in the computation. Considering the time history of the transversal force Fy on a rudder and compared to AP result, Fig. 9, it is clear that the propeller/rudder interactions are not correctly predicted with the RFM approach. On the other hand, although the predicted Fy force on the rudder is quite different between the AP and AD formulations, the predicted yaw angle as shown in figure 10 by the two methods is almost the same. This can be explained by the fact that the side force of the propeller induces an additional side force in the opposite direction both on the hull and on the rudder. Consequently, global yaw moment acting on the hull is almost the same, although the side force acting on the rudder is quite different.

The time histories of the yaw and the rudder angles are presented in Fig. 10 and Fig. 11. The control by

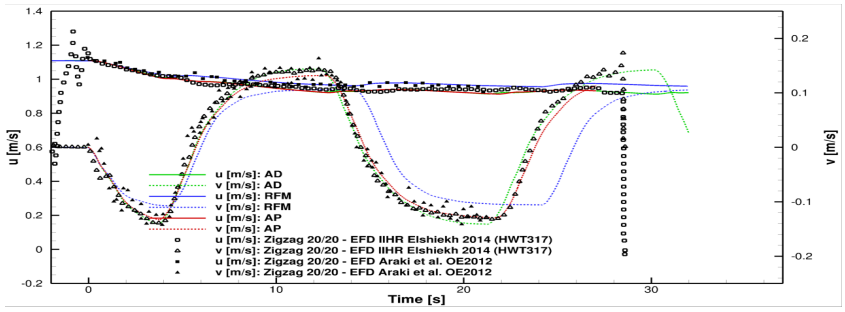

FIGURE 8 – Time history of the ship speed components (surge u, sway v)

RFM is systematically late while AD performs fine although slightly in advance on OS3 (a shorter time period). AP model performs nicely, in agreement with the EFD data. The time history of the roll angle is presented the same way in Fig. 12. There is a remarkable agreement between the prediction obtained by the AP model and the digitized EFD from [13], both in time and amplitude with all the main frequencies captured. Same conclusions hold for AD model with a motion period underestimated and in the opposite

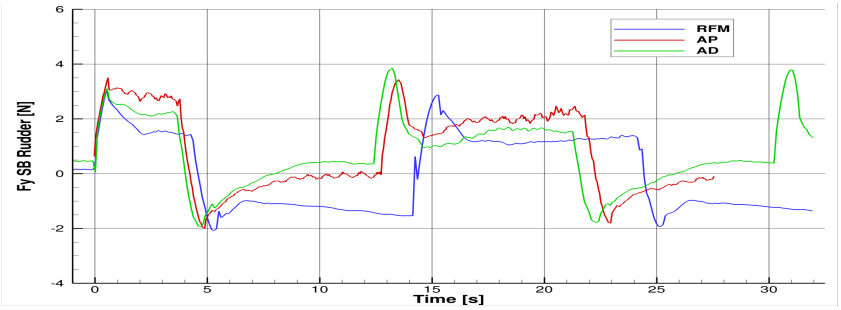

FIGURE 9 – Time history of transversal force Fy on the starboard rudder (in the frame linked to the rudder)

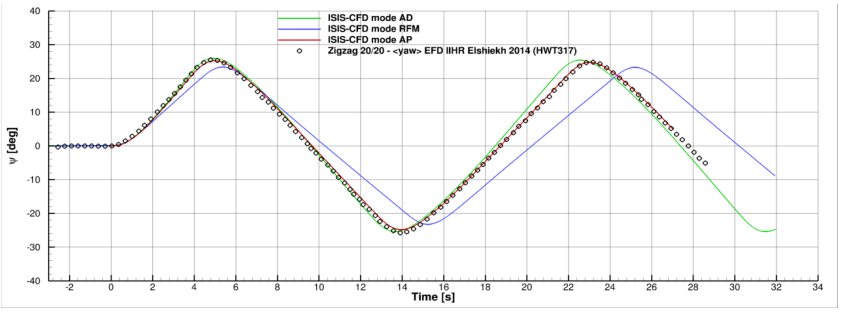

FIGURE 10 – Time history of the yaw angle

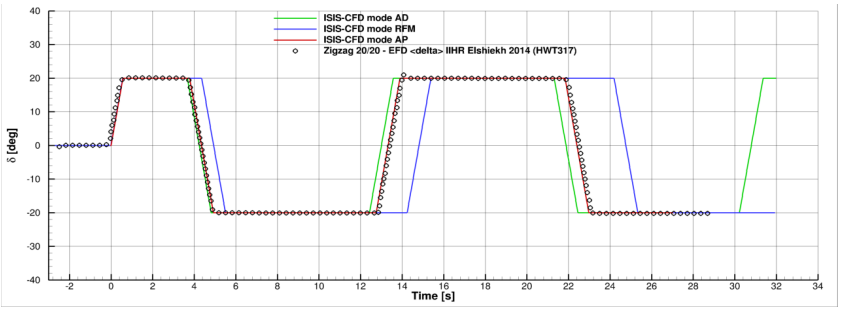

FIGURE 11 – Time history of the rudder angle

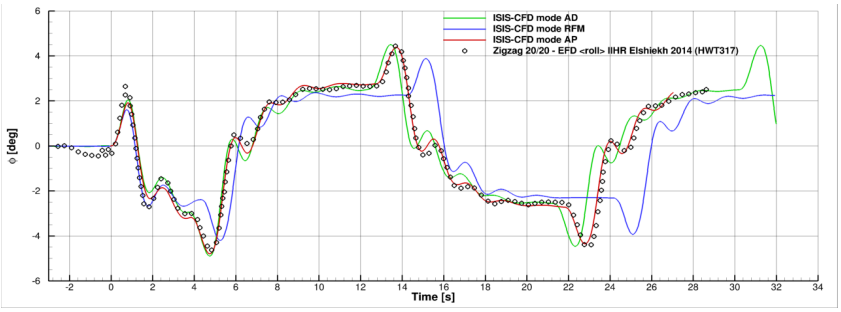

FIGURE 12 – Time history of the roll angle

for RFM. This is an indirect verification for the choice of the kxx inertia coefficient 0.34B (the proposed 0.344B would not change significantly the result).

An analysis of the flow details, correlated with motion and force histories, in order to understand the defaults of a propeller model and of physical modeling (turbulence) is extremely difficult to carry out here. As an example, Fig. 13 and Fig. 14 compare the instantaneous distributions of the axial velocity

and turbulence kinetic energy (TKE) in an horizontal plane through the propeller center at a time when the yaw returns to zero between OS1 and OS2 (see Fig. 5). The trace of high velocity region shown in figure 13 is the imprint of the drift angle. It can be seen from figure 13 that tha AP and the AD models give similar prediction, while the result obtained by the RFM approach suggests a lower drift angle. The AD model produces lower TKE levels than the resolved propeller. It is reminded that conventional linear eddy-viscosity type turbulence models fail to predict separated flow with accuracy. Here, if the flow in the propeller/rudder interaction is driven by the pressure with low occurrence of separation (to be confirmed) then it could explain why, although the TKE distributions are different, the AD model is still in line with the AP model. A better overview of flow details in that region can be accessed from this link with a video for the AP model : https ://www.youtube.com/watch ?v=5RpZexkz9pY.

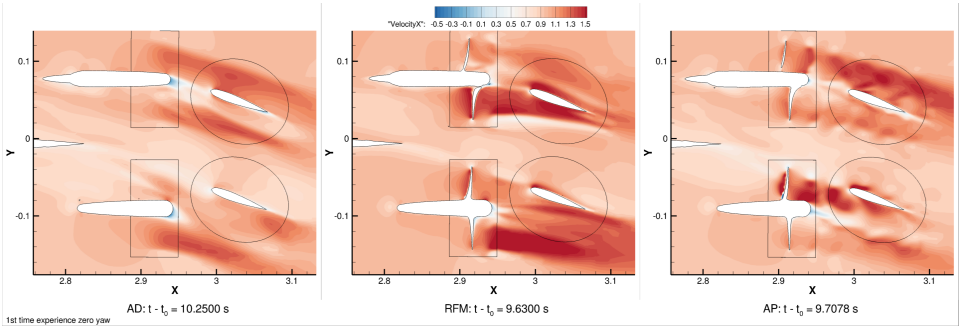

FIGURE 13 – Instantaneous contour distribution of axial velocity in a cut plane

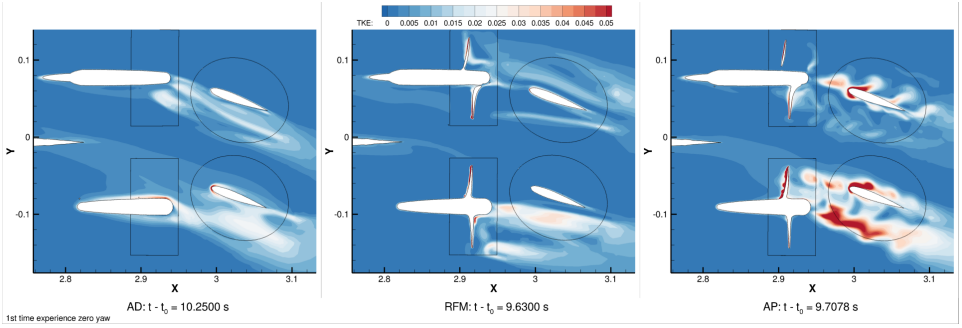

FIGURE 14 – Instantaneous contour distribution of the turbulence kinetic energy in a cut plane

6.3 KCS self-propulsion step

Similar to the ONRT test case, a self-propulsion simulation has been performed first to determine the propeller revolution speed used in the maneuvering simulation. The propeller rps is adjusted to match the model scale self-propulsion point with the target ship speed of 2.006m/s. The measurement data is n=11.41rps. The AD approach predicts n=11.65rps with 2.1% over prediction, while the AP approach gives a higher value n=11.94rps with 4.7% over prediction. We believe that the over prediction obtained by the AP approach is mainly due to turbulence modelization. At model scale, the flow near the leading edge of the blade is more likely in a transitional regime, while the RANSE model with wall function is employed in the CFD simulation in order to save CPU time. Consequently, the thickness of the turbulence boundary layer in the CFD simulation is higher, resulting in a lower propeller thrust and higher propeller torque. A higher propeller revolution rate is therefore needed to achieve the self-propulsion equilibrium.

6.4 KCS $20°/20°$ starboard side zigzag motion

The zigzag motion simulation for the KCS test case is performed with a setup similar to the ONRT test case. Since the prediction with the RFM approach is very poor, only the AD model and the AP model are compared for this test case. The predicted yaw angle is compared with the measurement data obtained by MARIN in figure 15. Compared to the previous test case, the CFD predictions are less satisfactory, especially with the AD model. Such behaviors can be attributed to the type of rudder. A semi-spade type of rudder is used in the KCS test case. The gaps between the mobile part and the fixed part of the rudder makes the flow separate more easily from the rudder even at small rudder deflection angle. As separated flows are usually not well predicted with RANSE turbulence model, more discrepancies are observed as expected.

The better prediction with the AP model can be attributed to its capability to take into account the ef-

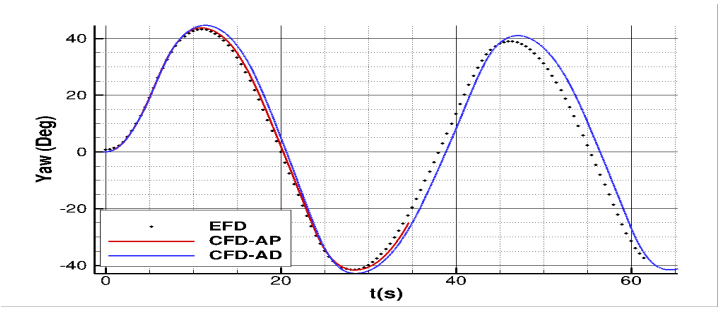

FIGURE 15 – Time history of yaw angle for the KCS zz2020 motion

fect of propeller side force. Before the second rudder execution, the propeller side force is acting in the opposite direction to the rudder side force as shown in figure 16. Moreover, it induces an additional side force in the opposite direction both on the rudder and on the hull. Consequently, both propeller models give similar prediction for the yaw angle. Shortly after the second rudder execution starting from t=6s, the direction of the propeller side force coincides with that of the rudder side force up to about t=12s when the drift angle changes the sign. During this period, propeller side force makes the ship turn faster compared to the case with AD model, resulting in a better prediction of the first overshoot angle. Later on, it is more difficult to analyse the effect of propeller side force. For instance, when the ship is at its maximum drift angle near t=20s, the difference on the side force predicted by two different propeller models on the hull is more important than the propeller side force. Moreover, propeller side force does not induce an additional side force on the rudder in the opposite direction as observed previously. There must be an interaction between the propeller side force and the flow separation around the rudder as well as the interaction with the longitudinal vortex developed along the hull.

The predicted roll angle is displayed in figure 17. Both propeller models are capable to provide a good prediction compared with measurement data with a better agreement observed with the AP model. However, it is difficult to extract more useful information from this comparison. The predicted surge velocity is compared in figure 18. It is observed that the AP model over predicts the surge velocity. By looking at the predicted surge force shown in figure 19, we can conclude that the over prediction of the surge velocity by the AP model is mainly due to a higher predicted propeller thrust at the beginning the zigzag motion. However, we do not think that this higher predicted propeller thrust is due to a poor prediction of the AP model, compared with the AD model. The reason of the over predicted surge velocity by the AP model is more likely due to the under-prediction of rudder resistance. The difference between the

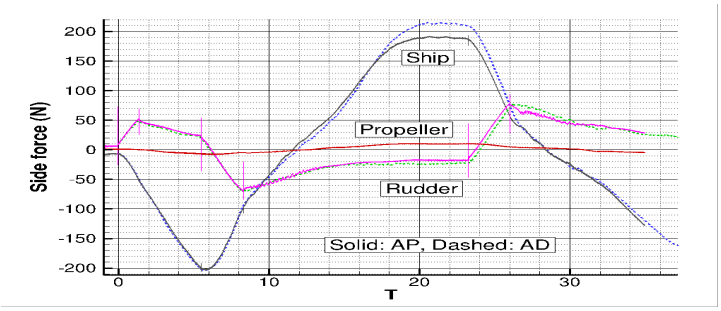

FIGURE 16 – Time history of side force for the KCS zz2020 motion

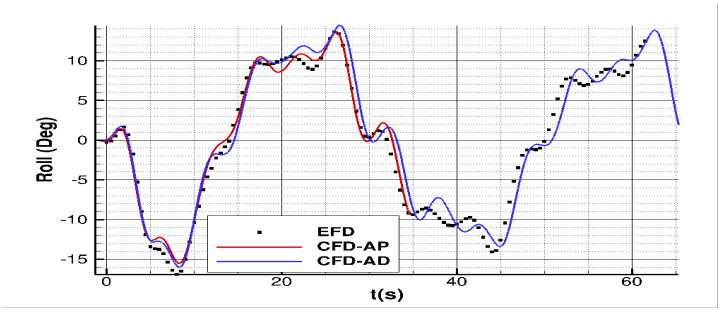

FIGURE 17 – Time history of roll angle for the KCS zz2020 motion

two propeller models on the surge force is also observed on the hull near t=20s when the drift angle is maximum. This observation suggests that there must be an interaction between the propeller and the longitudinal vortex developed along the hull which can not be captured by the body force model. Further investigation is needed. The drift angle is compared in figure 20. The measurement data is shifted down due to the initial condition. There is an initial yaw angle in the measurement before the zigzag motion starts which is not simulated in the computation.

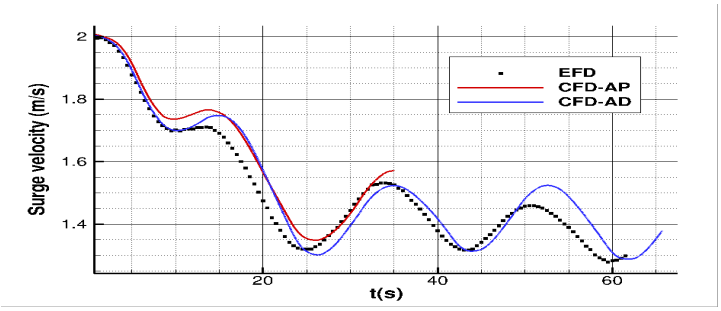

FIGURE 18 – Time history of surge velocity for the KCS zz2020 motion

6.5 KCS 35° starboard side turning circle motion

The initial condition of the turning circle motion is the same as the zigzag motion. Starting from the established self-propulsion solution, the rudder angle changes from 0° to 35° within 2.44755 seconds with a rudder rate of $14.3^\circ/s$. All 6 degrees of freedom of the ship are free. After a transient period, the flow reaches a steady state where all quantities in the ship coordinate system remain almost constant. The trajectory of the TC35 motion is displayed in figure 21. The predictions given by both propeller

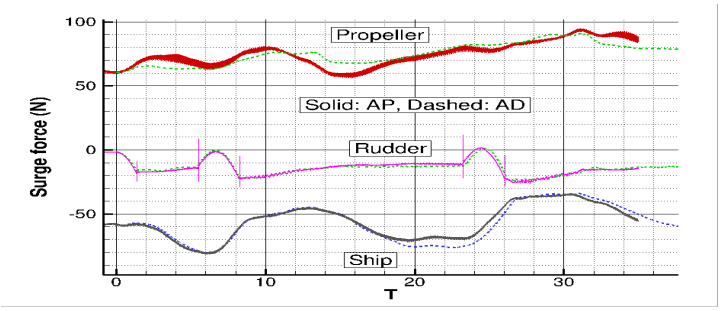

FIGURE 19 – Time history of surge force for the KCS zz2020 motion

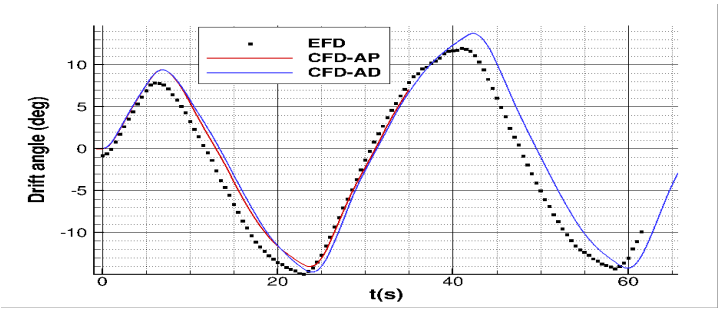

FIGURE 20 – Time history of drift angle for the KCS zz2020 motion

models are similar. The predicted radius for the steady gyration motion by the AP model is almost the same as the measurement data, while the AD model under predicts it by less than 2%. Both models suffer a common drawback compared with measurement result. The predicted yaw angle is noticeably smaller than the measurement result. Since the RANSE turbulence model under predicts the rudder side force at large rudder deflection angle as shown in a previous study [14], turbulence modelization error is expected to be the main cause of this deficiency. Another possible reason is the experimental condition. During this period, the ship model might be very close to the wall which might force the ship model to turn faster. Not shown in this paper, the port side turning circle simulation of the same case provides a much better agreement during this period. Numerical discretization error may also have a contribution since the mesh used in the present simulation is not very fine, and the AGR is used to capture the free surface and to ensure cell size continuity for the overset interface only. Further investigations are needed to quantify this error.

The predicted surge velocity is compared in figure 22. The prediction obtained by the AD model agrees well with the measurement data, while the AP model over predicts the surge velocity. To better understand the reason, the predicted surge force on the ship, on the rudder and on the propeller are compared in figure 23. The AP model predicts a higher propeller thrust. It induces a higher ship resistance as expected. The force acting on the hull and the propeller combined is higher during the transient period with the AP model, but they are almost identical at steady state. On the other hand, rudder resistance decreases rather than increases with the AP model. We believe that it is this under-estimation of rudder resistance due to turbulence modelization error that is responsible for the over estimation of surge velocity observed with the AP model.

The drift angle is compared in figure 24. CFD predictions agree well with the measurement during the transient period, but over predict the drift angle for the steady state. Since the relative rudder angle in the steady state is small which makes the CFD prediction for the flow around the rudder more accurate,

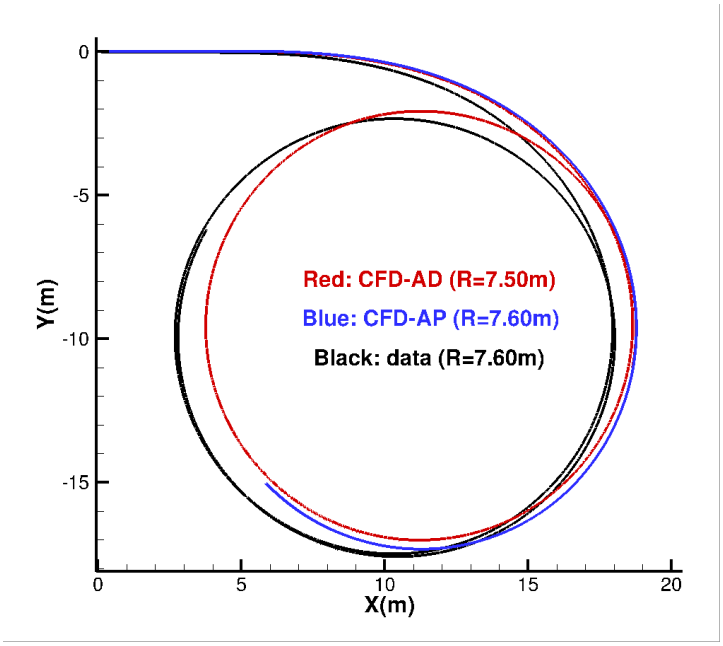

FIGURE 21 – Trajectory of the KCS TC35 motion

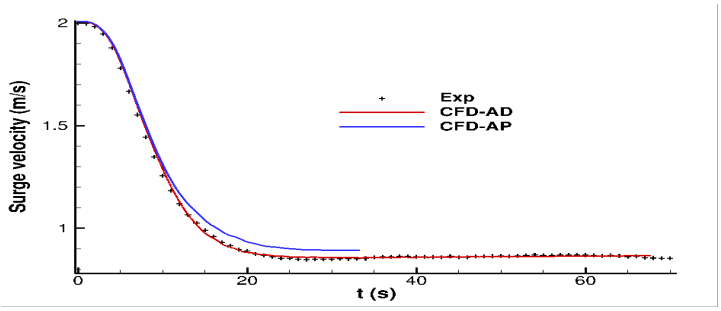

FIGURE 22 – Time history of surge velocity for the KCS TC35 motion

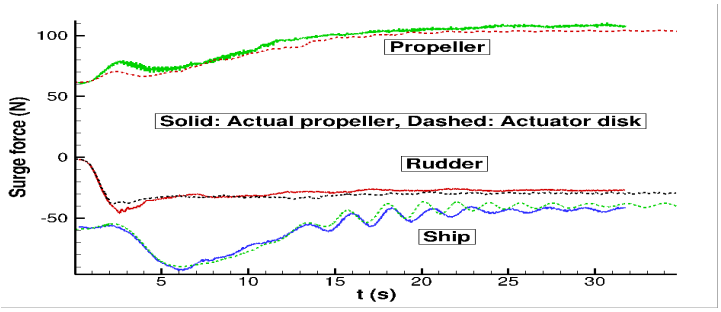

FIGURE 23 – Time history of surge force for the KCS TC35 motion

we believe that this discrepancy is due to the turbulence modelization error and spatial discretization error in the prediction of longitudinal vortex formed at the bow which is expected to be higher at high drift angle. Side forces acting on the hull, rudder and the propeller are compared in figure 25. It can be observed that the effect of propeller side force is limited for this test case. For completeness, CFD prediction for roll angle and yaw rate are compared in figure 26 and figure 27 respectively. It is however difficult to extract useful information from these comparisons.

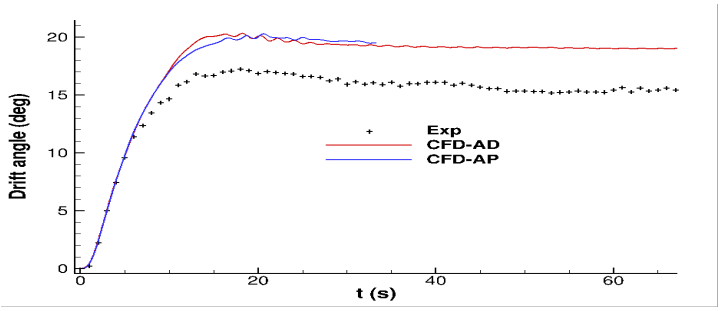

FIGURE 24 – Time history of drift angle for the KCS TC35 motion

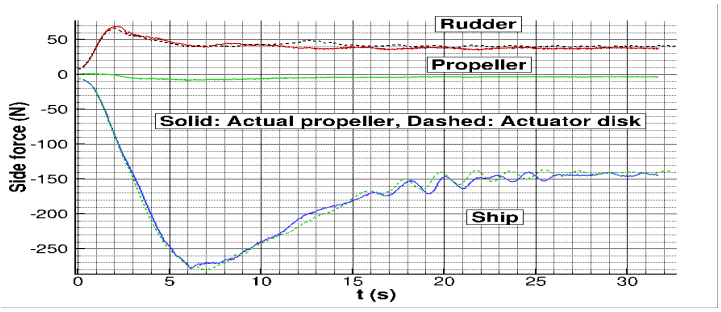

FIGURE 25 – Time history of side force for the KCS TC35 motion

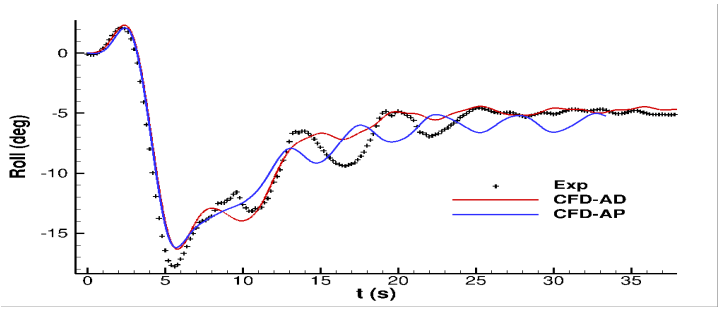

FIGURE 26 – Time history of roll angle for the KCS TC35 motion

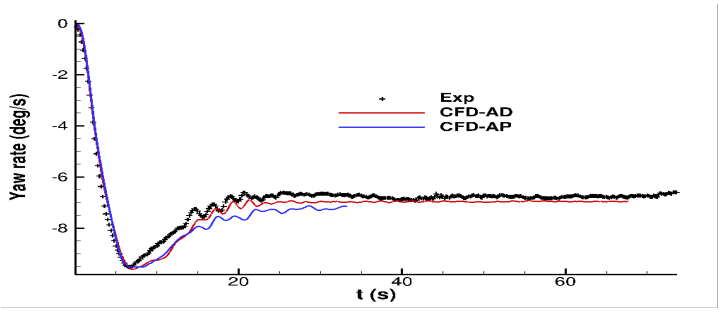

FIGURE 27 – Time history of yaw rate for the KCS TC35 motion

7 Conclusions

The zigzag and turning circle maneuvers have been computed for the ONRT and the KCS test cases with the help of the ISIS-CFD flow solver. The numerical setting for the study is considerably simplified by the use of the overset technology combined with anisotropic adaptive mesh refinement and de-refinement.

Three propeller models have been used and compared, from body force (AD) to a frozen-rotor like method (RFM) and with the actual propeller as a reference. The main conclusion is that the implemented AD model is cost effective, about 20 to 40 times faster compared to the propeller resolved simulations with a reasonable agreement between the two concerning the trajectory and the motions. A more accurate prediction is reached for the ONRT test case equipped with a spade type rudder. On the other hand, the RFM approach is unsuitable for such kind of simulation due to the poor prediction of propeller side force. While the propeller side force is correctly predicted by using the AP model, its effect has been found limited on the predicted motion, although the difference in the predicted forces and the moments on the rudder and the hull are noticeable. However, taking into account the propeller side force always results in an improved prediction. In addition to propeller model, turbulence modelization error for the prediction of the separated flow around the rudder at high rudder angle, especially for the semi-spade type propeller, as well as for the prediction of longitudinal vortex at high drift angle is also responsible for the discrepancies observed between the CFD simulation and the measurement.

Acknowledgements

This work was made possible thanks to granted access to the HPC resources of CINES and IDRIS computing centers under the allocation A0072A01308 made by GENCI (Grand Equipement National de Calcul Intensif). This work benefited also from access to the Centrale Nantes Supercomputing Centre's computing resources on Liger through the resource allocation OG1910290 granted by the Institut de Calcul Intensif (ICI).

Références

[1] E. Guilmineau, G.B. Deng, P. Queutey, M. Visonneau, A. Leroyer, J. Wackers, URANS simulations of planar motion mechanism for two hulls, Workshop on Verification and Validation of Ship Manoeuvering Simulation Methods (SIMMAN-2014) 2014.

[2] G.B. Deng, A. Leroyer, E. Guilmineau, P. Queutey, M. Visonneau, J. Wackers, A. del Toro Llorens, Verification and validation of resistance and propulsion computation, Proceedings of Tokyo 2015 - A Workshop on Numerical Ship Hydrodynamics, Tokyo, 2015.

[3] E. Guilmineau, G.B. Deng, A. Leroyer, P. Queutey, M. Visonneau, J. Wackers, Numerical Simulations for the Wake Prediction of a Marine Propeller in Straight-Ahead Flow and Oblique Flow, Journal of Fluid Engineering, No. FE-16-1574, Vol. 140(2), 021111-1, 2018.

[4] S. Bhushan, H. Yoon, F. Stern, E. Guilmineau, M. Visonneau, S. Toxopeus, C. Simonsen, S. Aram, S.-E. Kim, G. Grigoropoulos, Assessment of CFD for Surface Combatant 5415 at Straight Ahead and Static Drift $\beta = 20°$, Journal of Fluids Engineering, Vol. 141(5), 051101, 2019.

[5] P. Queutey, M. Visonneau, An Interface Capturing Method for Free-Surface Hydrodynamic Flows, Computers and Fluids, vol. 36, issue 9, pp 1482-1510, 2007.

[6] J. Wackers, B. Koren, H.C. Raven, A. van der Ploeg, A.R. Starke, G.B. Deng, P. Queutey, M. Visonneau, T. Hino, K. Ohashi, Free-Surface Viscous Flow Solution Methods for Naval Hydrodynamics, Archives of Computational Methods in Engineering, State of the Art Reviews (ARCME), Vol. 18, No. 1, pp 1-41, 2011.

[7] A. Hay, A. Leroyer, M. Visonneau, H-Adaptative Navier-Stokes Simulations of Free-Surface Flows Around Moving Bodies, Journal of Marine Science and Technology, vol. 11, pp. 1-18, 2006.

[8] P. Queutey, J. Wackers, A. Leroyer, G. Deng, E. Guilmineau, M. Visonneau, G. Hagesteijn, J. Brouwer, Dynamic behaviour of the loads of podded propellers in waves : experimental and numerical simulations, OMAE 2014, The 32nd International Conference on Ocean, Offshore and Arctic Engineering, 2014

[9] X. Gao, G.B. Deng, To evaluate the influence of DOF on maneuvering predictions by direct CFD zig simulations, VIII Int. Conference on Computational Methods in Marine Engineering, MARINE 2019, R. Bensow and J. Ringsberg (Eds), 2019.

[10] J. Wackers, G.B. Deng, A. Leroyer, P. Queutey, M. Visonneau, Adaptive grid refinement for hydrodynamic flows, Computers & Fluids, vol. 55, pp 85-100, 2012.

[11] J. Wackers, G.B. Deng, E. Guilmineau, A. Leroyer, P. Queutey, M. Visonneau, Combined refinement criteria for anisotropic grid refinement in free-surface flow simulation, Computers and Fluids, vol. 92, pp 209-222, 2014.

[12] M. Araki, H. Sadat-Hosseini, Y. Sanada, K. Tanimoto, N. Umeda, F. Stern, Estimating maneuvering coefficients using system identification methods with experimental, system-based, and CFD free-running trial data, Ocean Engineering, vol. 51, pp 64-84, 2012.

[13] H.A. Elshiekh, Maneuvering characteristics in calm water and regular waves for ONR Tumblehome, Master Thesis at the University of Iowa, Spring 2014.

[14] G.B. Deng, A. Leroyer, E. Guilmineau, P. Queutey, M. Visonneau, J. Wackers, Effect of Turbulence Modelization in Hull-Rudder Interaction Simulation, The 30th China Hydrodynamics Conference, Shanghai, China, August 2019.